

# Stable Vortex Configurations in a Cylinder

R.J. Zieve and L.A.K. Donev

*Physics Department, University of California at Davis*

We calculate stable arrangements for a single superfluid vortex pinned to the wall of a stationary cylindrical container. We find that, independent of the details of the pinning site, stable vortices must subtend most of the cell horizontally and cannot be vertical or nearly vertical. More generally, the geometry of a container severely limits the possible vortex configurations, making macroscopic trapped vortices less common than previously believed.

Vortex lines in superfluid helium have been studied for over forty years [1], but many fundamental questions remain. Moving vortices feel a drag force, known as mutual friction, from interaction with the superfluid excitations. The effects of mutual friction have been thoroughly measured in systems of many vortices [2], but there is still no microscopic theory of the interaction. Similarly, the interaction of two closely approaching vortex lines is unknown. Another unresolved issue is the structure of the vortex core, and whether it can change size and shape to alter the energy and momentum of a vortex. Other questions involve superfluid turbulence, which can be described as a tangle of vortex lines. In a decaying tangle, the mean vorticity has the same power-law dependence on time as for a classical system, even at such low temperatures that the normal fluid density is negligible [3, 4]. In addition, experiments [5] and simulations [6] show that superfluid turbulence follows a Kolmogorov scaling law at low temperatures. The power law, prefactor, and even the deviations from ideal scaling are the same for superfluid and classical turbulence. How the quantized vortices in the superfluid mimic so well the behavior of classical viscous vortices is unknown, as is the length scale at which differences appear. A better understanding of single vortex behavior may help answer these

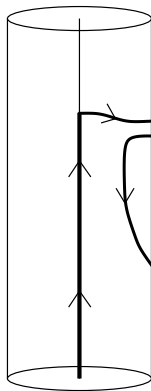


FIG. 1: Vortex partially trapped around a wire. The picture illustrates the possible interaction of the vortex with a second vortex pinned to the wall of the chamber.

questions.

A few years ago, an unusual method for observing vortex motion was discovered [7, 8]. A vortex line is partially trapped around a thin wire, continuing through the fluid as a free vortex, as shown in Figure 1. Although the vorticity is initially created by rotating the cryostat, the circulation around the wire is long-lived, and measurements can be made after the cryostat is brought to rest. In the case of a vortex partially attached to the wire, the self-velocity drives the free end around the cell. Its motion is detected through changes in the normal modes of the wire's vibration, which can identify the position where the free end attaches to the wire to within 1% of the wire length. The system also lends itself to computer simulation, with detailed computations of the vortex motion showing excellent agreement with the experimental data [9]. The vibrating wire technique allows direct investigation of how a single vortex interacts with various situations, including other vortices in the container, heat pulses, geometrical obstructions, or fluid flow across the cell. One of the simplest interactions is with a single additional vortex line, pinned to the cell wall in a metastable configuration. The work discussed here began as an attempt to identify metastable vortex configurations for use in the experiments. Since the measurements, unlike most vortex studies, will be made with the cryostat stationary, we use this situation in our calculations. From here on, we refer to metastable pinned vortices in a stationary cylinder as "stable." We find that the only stable single vortex configurations are mainly horizontal, an orientation that may be difficult to achieve after rotation around a vertical axis. This result may be part of the reason for the smooth vortex motion observed in the experiments: the vortex line is not perturbed by interactions with macroscopic pinned vortices because few if any such vortices are present.

## I. VORTEX CONFIGURATIONS

We test for stability with a computer program along the lines of Schwarz's code for modeling vortex dynamics [10]. The equations used are discussed at length in Ref. [10], and in subsequent work by other groups [11, 12, 13, 14? ], so they are summarized only briefly here. We treat the vortex cores

as massless and thin; that is, the core diameter is small compared to the curvature along the core. The equation governing the motion of superfluid vortices is essentially the Euler equation for incompressible fluid flow, with an additional term for mutual friction between the vortices and normal fluid. Physically, in the absence of friction, the vortex cores move at the local superfluid velocity. In our code, a set of points along a vortex core is stepped through time, with the velocity  $\dot{\mathbf{s}}$  of a point on the core given by  $\dot{\mathbf{s}} = \dot{\mathbf{s}}_o + \alpha(\dot{\mathbf{s}}_o \times \mathbf{s}')$ , where

$$\dot{\mathbf{s}}_o = \frac{\kappa}{4\pi} \int' \frac{(\mathbf{s}_1 - \mathbf{s}) \times d\mathbf{s}_1}{|\mathbf{s}_1 - \mathbf{s}|^3} + \frac{\kappa}{4\pi} \ln \frac{2\sqrt{l_+l_-}}{e^{1/4}a_o} (\mathbf{s}' \times \mathbf{s}'') \\ + \mathbf{v}_a + \mathbf{v}_b.$$

Here  $\alpha$  is a friction coefficient,  $\kappa$  is the quantum of circulation, and  $a_o$  is the radius of the vortex core. In  ${}^4\text{He}$ ,  $\kappa = 9.98 \times 10^{-4} \text{ cm}^2/\text{s}$  and  $a_o = 1.3 \times 10^{-8} \text{ cm}$ . The first term integrates over the vortex core to find the contribution to velocity of the non-local parts of the vortex. We approximate the core as linear between each pair of specified points. When calculating this term at a given point, we omit the vortex segments on either side of that point. These segments, of lengths  $l_-$  and  $l_+$ , instead contribute to the second term, which arises from the local curvature,  $R$ .  $\mathbf{s}'$  is the unit vector along the direction of the vortex core, and  $\mathbf{s}''$  is a vector of length  $1/R$ , directed toward the center of curvature. The applied velocity is  $\mathbf{v}_a$ ; in our work this comes from either a vertical vortex located at the center of the cylinder, or a constant vertical velocity. The boundary field  $\mathbf{v}_b$  satisfies  $\nabla^2 \mathbf{v}_b = 0$  everywhere inside the cylinder, and must cancel the perpendicular velocity at the cell wall from the other terms to ensure that the entire velocity field has no perpendicular component at the wall.

Before presenting our program and results, we briefly discuss vortex pinning. A standard picture is that surface roughness can pin a vortex by providing a local minimum in the vortex's length, and hence in its energy. Schwarz gave this intuition numerical support by showing that a hemispherical bump on an infinite plate will trap one end of a half-infinite vortex line [16]. His work includes no explicit pinning term in the equations of motion; the important point is that the geometry itself can catch the vortex line. As the vortex moves nearby, the distortion of the fluid flow by the bump directs the vortex towards the bump. The vortex typically spirals around the bump before reaching a stationary configuration. The particular geometry used allows an exact solution to Laplace's equation using image vortices. Furthermore, two bumps on opposing parallel walls pin vortices [10]. That is, a vortex with its endpoints on the two bumps will reach a stable position even if there is an imposed superfluid flow between the plates. At some critical velocity, the vortex comes off the bumps and is swept along by the flow. Without the pinning sites, the vortex would always move with the flow.

As an example of pinning sites that do not support a stable vortex, consider two bumps on an infinite plane, as shown in Figure 2. A vortex arching in a semicircle between the bumps, with its image vortex, forms a ring. Its own velocity pushes it along its axis, but with the ends pinned the vortex and image collapse towards each other. They then attract each other

more strongly, and the vortex eventually hits the wall and annihilates.

More generally, a vortex pinned in any container will be attracted to the nearest wall. The velocity contribution of the vortex itself may cancel the influence of the wall, resulting in a stable vortex configuration, but whether this happens depends on the container shape and the locations of the vortex endpoints. Here we find the possible stable vortices terminating on the curved walls of a cylinder. Except when otherwise stated, the calculations use a cell of radius 0.01 cm and length 0.5 cm.

## II. NUMERICAL CONSIDERATIONS

We use a fifth-order Runge-Kutta-Felberg method with a variable time step for solving the ordinary differential equation. The step size is determined by the relative difference between the fourth-order and fifth-order steps, except that when the velocity is very small the absolute difference is used instead. This greatly improves stability and eliminates the need for the hopscotch algorithm Schwarz cites [10]. With our code, a vortex ring of radius 0.01 cm propagates for hundreds of centimeters without noticeable distortion, even in the absence of friction. The time step is about  $2.5 \times 10^{-3}$  seconds for 25 points along the vortex core. The time step is limited by stiffness and is roughly quadratic in the minimum point spacing, so using a stiffly stable method (e.g., backward Euler) could allow a larger time step. By contrast, without friction Schwarz could propagate a vortex this size only 0.7 cm before an instability appeared with a time step of  $2 \times 10^{-4}$  seconds, and this distance decreases with longer time steps [10]. A similar improvement in performance was noted with a Crank-Nicolson algorithm and variable time step [? ]. As a test case for stability of various algorithms, Aarts [? ] considers a distortion with period two points on either a vortex ring or a straight vortex. Even with no mutual friction, these distortions do not grow with our algorithm.

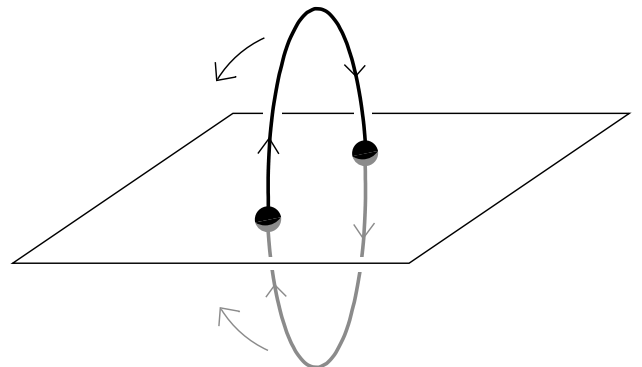


FIG. 2: Vortex with both ends pinned to bumps on an infinite plane. The vortex (black) and its image (gray) attract each other and ultimately annihilate.

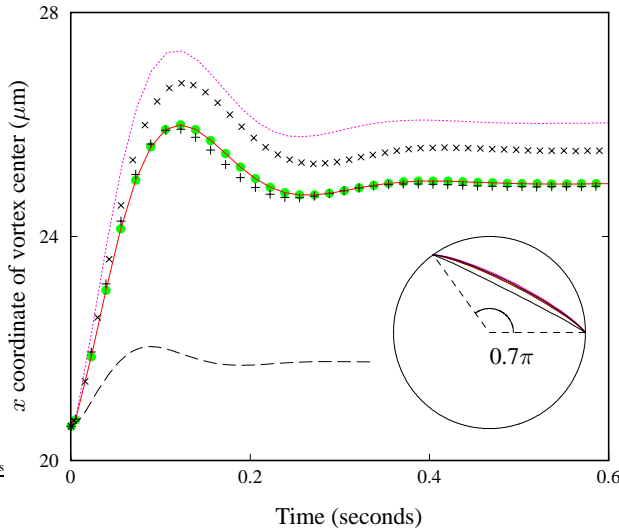


FIG. 3: Motion of the middle of a vortex line, calculated using different boundary treatments. All use  $\alpha = 0.5$  and cell radius 0.01 cm, and all but the solid line have cell height 0.5 cm. The symbols show inversion images followed by Fourier transforms on a  $16 \times 16$  (x),  $32 \times 32$  (●), or  $64 \times 64$  (+) grid. The lines show inversion images only (dotted), infinite radial continuations of vortices (dashed), and inversion images with Fourier transforms on a  $64 \times 64$  grid for a cylinder 1 cm long (solid). The inset shows the corresponding final configurations.

A minor difference in the calculation is that Schwarz approximates vortex segments by the circle passing through three consecutive points. We do use the radius of this circle as the local curvature of the vortex line. However, rather than calculating the tangent to the circle, we use the vector between a point's nearest neighbors as the direction of the vortex at that point. We note that even using the exact tangent to the inscribed circle provides a consistent picture of the vortex line only locally, since the local calculations for two consecutive points assume different shapes for the intermediate segment. Since the tangent vector is used only to define the direction of the friction contribution to the vortex motion, our approximation is identical to that of Schwarz for a stationary configuration. The two are nearly equivalent even for vortex dynamics except in situations of uneven point spacing or sharp bends. We did verify with a direct calculation that our numerics are essentially independent of this calculational detail.

We make one departure from the differential equations by subtracting the velocity tangent to the vortex core before updating the configuration. This prevents points along the vortex line from drifting towards one end of the line. We believe this is reasonable even for dynamical simulations, and it definitely should not affect the equilibrium configurations we discuss here. Since our vortices are nearly stationary, the point spacing remains constant to within a few percent once we neglect the tangential velocity component. Our code checks the point spacings at each time step, and can add or delete points to keep

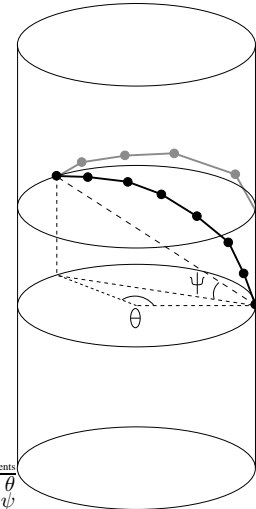


FIG. 4: Construction of image vortices for cylinder by inversion. The vortex (black) ends on the cell wall. The nodes are separately inverted, and their images define the core of the image vortex (gray). The angle  $\theta$  is the horizontal separation of the vortex endpoints, measured from the cylinder axis. The angle from the horizontal of the line connecting the endpoints is  $\psi$ .

the spacings uniform. No points were ever added or deleted during the computations presented here.

For many purposes, the boundary contribution  $\mathbf{v}_b$  to the velocity field can be ignored. However, stability depends heavily on the flow field near the container wall, where  $\mathbf{v}_b$  can be significant. As an illustration, Figure 3 compares the motion of the center of a vortex line for several different treatments of the boundary. The pin sites lie in a horizontal plane at the center of the cylinder, and are separated by an angle  $\theta = 0.7\pi$ . Straight radial extensions of the vortices are the furthest from giving a vanishing perpendicular velocity at the walls, and result in substantially different motion from the other treatments. Assigning images by inversion is a better approximation. The original vortex is described by discrete points along its core. As shown in Figure 4, we invert each of these points in a horizontal circle with the same radius  $R_c$  as the cylinder. Thus, in cylindrical coordinates,  $(\rho, \theta, z)$  maps to  $(R_c^2/\rho, \theta, z)$ . These image points are then used to describe the core of a new vortex line. In this way any vortex with both ends terminating on the cell wall becomes, with its image, a closed loop. Since the image vortices give only an approximate solution, we then use a Fourier series solution of Laplace's equation to cancel any remaining perpendicular velocity at the curved wall. We calculate the perpendicular velocity arising from the real and image vortices at a grid of points on the curved surface of the cylinder. We do a two-dimensional discrete Fourier transform of these velocities to get the coefficients of a Fourier series solution of the boundary value problem. Subtracting this solution from the other velocity contributions helps meet the boundary condition. An infinite Fourier series would give the unique solution to the

fluid velocity for the given vortex core arrangement, but the discrete Fourier transform we use can be only an approximation. The perpendicular velocity is cancelled exactly at the grid points and approximately between points. Figure 3 shows results from several grid spacings. As the Fourier grid becomes finer, the combination of inversion images and Fourier solutions converges. We do not reduce the grid size beyond the point spacing along the vortex core. We assume there is no flow through the top and bottom faces of the cylinder, a reasonable approximation as long as the vortices are far from the ends. The solid curve of Figure 3, which represents calculations in a longer cylinder, verifies that we are in the regime where vortex motion does not depend on cell length, and justifies our neglect of the ends. The  $xy$  projection of the final vortex configurations for the various treatments are shown in the inset of Figure 3. Except for the straight vortex continuations, the final arrangements cannot be resolved on the scale of the graph.

To study pinning, one might introduce bumps on the wall of a cylinder and work with the resulting boundary field. With this approach, the point spacing along the vortex would have to be small compared to the bump size, and the boundary solution would be complicated by the bumps themselves. Instead,

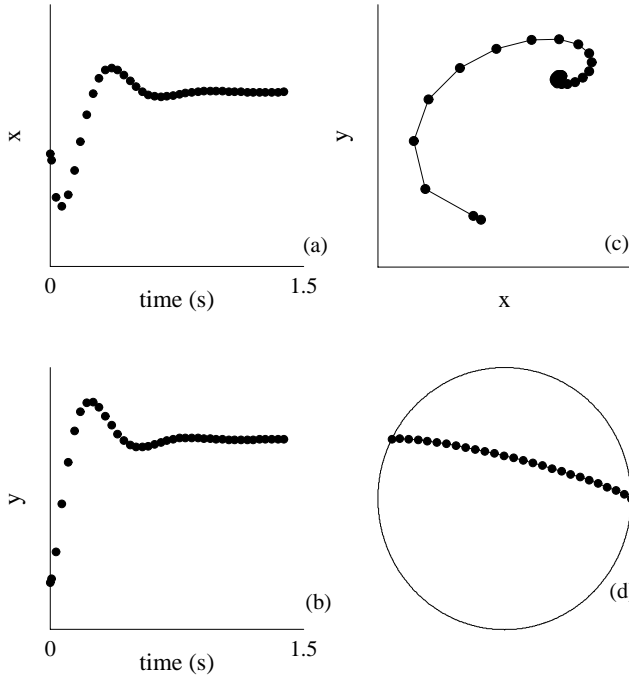


FIG. 5: Vortex line settling into a stable configuration. The  $x$  and  $y$  coordinates of the middle of the vortex line both show damped oscillations as a function of time in (a) and (b). In (c), the projection of the middle of the vortex onto the  $z = 0$  plane, parametrized by time, spirals towards its equilibrium position. Finally, (d) shows the projection onto the  $z = 0$  plane of the cylinder and the final vortex configuration. The pin sites are at an angle of  $0.85\pi$  in the  $z = 0$  plane and at an angle of  $0.25\pi$  from the horizontal, and the friction coefficient is  $\alpha = 0.5$ .

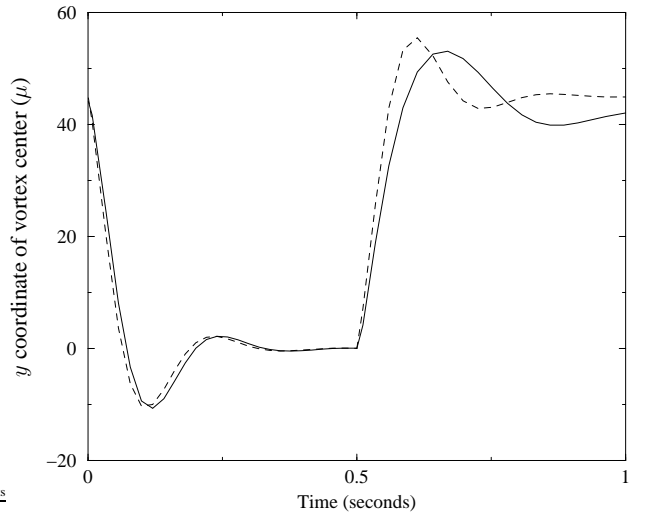


FIG. 6: Decaying oscillations on a vortex stretched between two planes. The plane separation is 0.02 cm, the friction coefficient is 0.5, and there are 25 evenly spaced points along the vortex. The applied velocity is zero up to 0.5 seconds and  $-0.7 \text{ cm/s}$  in the  $x$  direction thereafter. The dashed lines represent the analytic solution for waves on a straight vortex.

we impose pinning externally, requiring that the endpoints of the vortex remain fixed at certain points on the cylinder wall. We then use a relatively large point spacing. As long as the size of the pin site is small compared to the point spacing, the lack of detail near the site should not affect the vortex behavior. After describing typical stable and unstable vortex behavior, we will present additional justification of this procedure.

When the chosen endpoints support a stable configuration, the vortex line spirals towards it. Figure 5 shows the behavior of a vortex as it moves toward a stable arrangement, and the final vortex configuration. Tracking the location of a given point on the core as a function of time shows decaying oscillations in each coordinate. These oscillations are the lowest frequency Kelvin waves. For an infinite straight vortex, the mode with wavelength  $k$  has  $\omega = \kappa k^2 A / 4\pi$ , where  $A \approx \ln(\frac{1}{ka})$ , and time constant  $\tau = 1/\alpha\omega$  [15]. In Figure 5, the oscillations have  $\omega = 10.76 \text{ rad/s}$  and decrease in amplitude by a factor of 0.0436 per cycle. Since the endpoint separation is 0.026 cm, the lowest mode has  $k = \pi/0.026 = 120 \text{ cm}^{-1}$ , corresponding to  $\omega = 15.48 \text{ rad/s}$  and damping of  $e^{-\pi} = 0.0432$  per cycle.

The damping per cycle is in excellent agreement with theory, and the discrepancy in the frequencies arises from boundary effects. We find a similar effect for the parallel plane geometry, as shown in Figure 6. Up to time 0.5 seconds, there is no applied velocity field. The vortex line is initially bent, in its equilibrium configuration for a constant applied velocity  $-0.7\hat{x} \text{ cm/s}$ . The first oscillations show the return of the vortex to vertical. The  $y$ -coordinate of the vortex center is shown. At time 0.5 seconds the applied velocity is changed to  $-0.7\hat{x} \text{ cm/s}$ , and the subsequent oscillations show the vortex settling

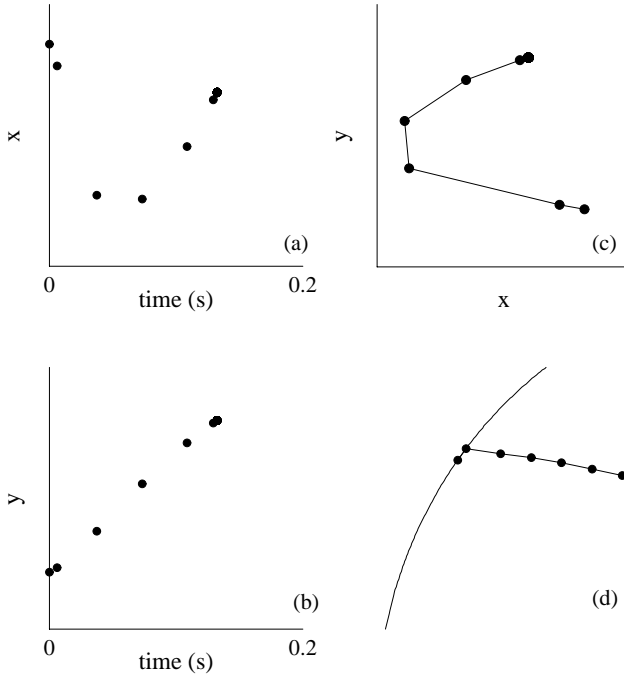


FIG. 7: Vortex line being pulled into wall. As a function of time, the  $x$ -coordinate of the middle of the vortex (a) appears to begin oscillating. However, the  $y$ -coordinate (b) moves steadily in one direction. At a time less than 0.2 seconds, the time step becomes too small to observe further time evolution. In (c) the  $z = 0$  projection, parametrized by time, is shown. Part (d) shows the portion of the final configuration near one of the cylinder walls, with the first segment of the vortex pulled against the wall. The pin sites are at an angle of  $0.8\pi$  in the  $z = 0$  plane and at an angle of  $0.27\pi$  from the horizontal, and the friction coefficient is  $\alpha = 0.5$ .

into a bent configuration. The frequency is significantly faster in the first half second, when the vortex is oscillating around a straight line. The dotted lines show the exponentially damped oscillations expected from the analytic solution for waves on a straight vortex, with the initial amplitude matched to the simulations and no other adjustable parameters. The remaining discrepancy in the first half second arises because the image vortices needed to meet the parallel plane boundary conditions result in a scalloped extension of the vortex, rather than a vortex with a sinusoidal distortion. For a nearly straight vortex, the two differ only slightly, while for the bent vortex the difference is more significant. We have checked that our simulations for waves on a long free vortex do agree with the analytic dispersion relation. Thus we are confident that the observed decrease in frequency for the pinned vortex in a cylinder is caused by the boundary and the vortex curvature.

The damped Kelvin oscillations of Figure 5 appear only for certain endpoint positions. For other locations at least one coordinate shows no oscillations, and the time step decreases until it reaches the minimum allowed value. After this, the progression in time is so slow that the further development of the vortex cannot be reached. Figure 7 illustrates this possibil-

ity. The final point shown in each of the first two parts of the figure is actually a large number of data points, which cannot be distinguished because of the small time step. Examining the calculation at each point shows that the time step crash arises near where the vortex joins the wall. The velocity at this spot becomes large and strongly dependent on the exact configuration. Often, in fact, part of the core tries to move through the cylinder wall. We interpret the time step crash as indicating that an actual vortex line would be pulled into the wall by its image vortex until it eventually annihilated or freed itself from the pin site. Thus the time step crash indicates an unstable pin configuration. If we were using bumps on the cylinder wall as pin sites instead of externally imposed pinning, the end of the vortex would move along the bump until reaching the cylindrical wall, and would then continue along the cylinder.

We tested our treatment of the pin centers in a configuration of two parallel planes. For this geometry an infinite series of image vortices would give an exact solution to the boundary conditions for the fluid flow. We sum the series out to ten times the plane spacing, and from there we continue the vortices to infinity as straight lines perpendicular to the planes. Schwarz carried out parallel plane calculations with hemispherical bumps, no external pinning, and a point spacing small compared to bump size. He found that the critical velocity for the vortex to remain on a bump was given by

$$v_c = \frac{\kappa}{2\pi D} \ln \frac{b}{a_o},$$

with  $D$  the spacing between planes and  $b$  the bump radius [10]. Using externally imposed pinning, we also find that a vortex with one end pinned to each plane reaches a stable configuration as long as the fluid velocity between the planes is sufficiently small. For large fluid velocities, we instead observe the time crash behavior described earlier, with the vortex attempting to move through the walls. The crossover between the two regimes defines a critical velocity, which depends on the vortex point spacing near the walls but not on the point spacing midway between the planes. Our observation of the vortex crashing into the wall is consistent with earlier work that assumed a vortex becomes parallel to the wall at the critical velocity [17]. A numerical solution of the Hall-Vinen-Bekarevich-Khalatnikov equations, setting vorticity parallel to the wall as a boundary condition, gave good agreement with experimental results on pinning in rough channels [17].

Our own approximation has the following interpretation. For a given applied velocity, any bump with radius larger than some value  $b_1$  would pin the vortex. In addition, for a given point spacing, we can only expect reasonable results for bumps smaller than some other value  $b_2$ , which we expect to be on the order of the point spacing. For larger bumps, our neglect of the distortion of the flow field near the bump will lead to incorrect behavior. If  $b_1 < b_2$ , then our program can do a realistic treatment of a bump of size  $b$  with  $b_1 < b < b_2$  and find a stable equilibrium position of the vortex. On the other hand, if  $b_1 > b_2$ , then any bump treated reasonably by our program would fail to pin the vortex. Since the program

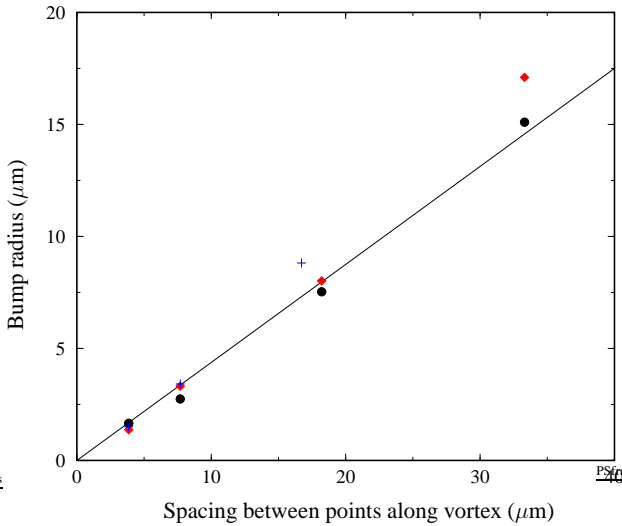


FIG. 8: Bump radii with the same critical velocity as various point spacings. The critical velocities were calculated for a vortex pinned between parallel planes of separation 0.01 cm (+), 0.02 cm ( $\diamond$ ), and 0.04 cm (●). The line is a guide to the eye.

enforces pinning, the result is an unphysical crash of the vortex into the wall. To model the effects of a larger bump, we would have to increase the spacing between our points.

To estimate the bump size corresponding to a given point spacing, we use the parallel plane geometry. We identify a point spacing with the bump size which yields the same critical velocity, using Schwarz's formula to convert bump size to critical velocity. We use the initial point spacing along the vortex, but the spacing typically changes by less than 5% during a calculation. Figure 8 shows this relationship between bump size and point spacing, for three different plane separations. The points lie close to a line of slope 0.4, with significant deviations only when the point spacing becomes too large relative to the plane separation. As long as the point spacing is much smaller than the plane separation, the plane separation does not change the effective bump radius, giving some confidence that the same correspondence will hold in a cylindrical geometry as well. Most of the results here correspond to bumps of radius about 3  $\mu\text{m}$  in our cylinder of radius 100  $\mu\text{m}$ .

As an additional check on our treatment of bump size and point spacing, we have run simulations of a vortex pinned between parallel planes, with hemispherical bumps as described by Schwarz [16]. The plane separation is 0.02 cm, and the bump has radius 7.8  $\mu\text{m}$ . We use point spacing 0.63  $\mu\text{m}$  near the bump, and the friction coefficient is 0.5. The solid circles of Figure 9 show one component of the motion of the vortex line's midpoint. We then repeated the calculation without the bumps, but with imposed pinning. The lines of Figure 9 represent three different point spacings: from lowest to highest, 25  $\mu\text{m}$ , 18  $\mu\text{m}$ , and 12.5  $\mu\text{m}$ . By our critical velocity matching criterion, the second of these corresponds to a bump radius

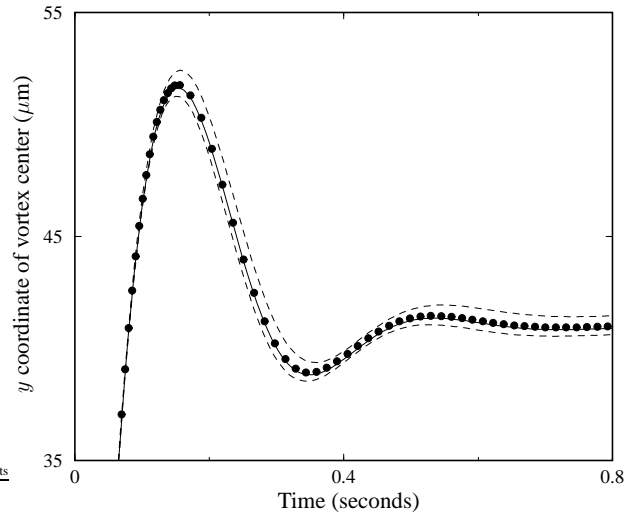


FIG. 9: Comparison of dynamics for real bumps and for imposed pinning. The motion of the middle of a vortex line is shown. The points show the behavior for actual bumps. The solid line is for imposed pinning, with point spacing corresponding to the same bump size. The two dashed lines are for slightly larger and smaller point spacings.

of 7.8  $\mu\text{m}$ ; and indeed, the middle, solid trajectory runs very close to the circles. The other point spacings yield the dashed lines, which are noticeably further from the path of the vortex on the actual bump. This demonstrates that our proposed correspondence between point spacing and bump size gives the correct dynamical behavior far from the pinning site.

Our final deviation from the ideal equation is that in finding equilibrium states, we use an unphysically large friction coefficient. Thus the calculated path of the vortex line as it settles to an equilibrium position does not correspond to real vortex dynamics in superfluid helium at low temperature. The final situation, however, should be unaffected. The one exception is that a too-low friction coefficient can lead to a time step crash when a vortex overshoots its equilibrium configuration while spiraling into position. In this situation the friction value is not merely an artifact of the numerics. Low friction could also lead to a real vortex line's being unable to reach a stable position. As shown in Figure 10, this is a small effect, changing the boundaries of the stable regime by only a few percent for a friction coefficient of at least 0.5. In the data discussed below we use the large-friction limit, since our concern is to find ultimately stable vortex positions. In our actual experiment, with rotation and with many vortices present in the cell, the conditions for trapping a vortex will be much more complicated than the present calculations. For most tests we use a straight vortex as the initial configuration, but we have also used parabolic vortices, and scaled versions of stable vortices. The different initial conditions yield the same ultimate stable configurations and the same dividing line between stable and unstable.

### III. RESULTS AND DISCUSSION

In the vertical direction, in which a cylinder has no curvature, all vortices are unstable. As might be expected, the vortices suffer the same fate as vortex arches on a plane. For horizontal vortices, there is a regime of stability when the vortex spans much of the cell; for example, a vortex running along a diameter is stable. As the angle subtended by the vortex decreases, the attraction to the cylinder wall grows stronger until the configurations become unstable. Introducing any vertical displacement between the pin sites quickly reduces the stability. Figure 10 shows the stability regime for our typical point spacing of about  $7.7 \mu\text{m}$ , corresponding to a bump radius of about  $3 \mu\text{m}$ . The effects of changing the friction coefficient or point spacing are also shown. The larger point spacing is about  $33 \mu\text{m}$ , corresponding to a  $17 \mu\text{m}$  bump radius. For larger point spacings, we cannot expect meaningful results because the spacing is no longer “small” compared to the cell radius. For smaller spacings, an isolated bump of the corresponding size is too small to be constructed in the physical experiments.

In the planned experiments, a single vortex will be trapped around a vertical wire near the middle of the cylinder. Thus, in Figure 11 we examine the stability of the trapped vortex line in the presence of a vortex along the  $z$  axis. The central vortex has a noticeable effect on stability. In the most likely configuration, the central vortex and the vertical component of circulation of the pinned vortex have the same direction. Since the two vortices repel each other, the loop is attracted more strongly towards the wall and destabilized. However, if

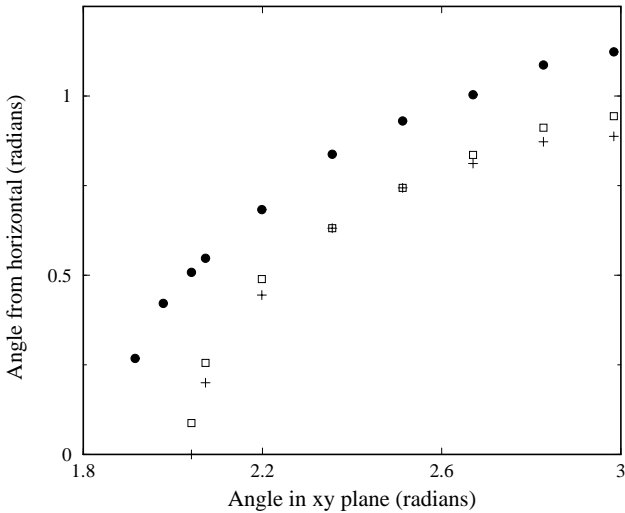


FIG. 10: Stable regime for single vortex in cylinder of height  $0.5 \text{ cm}$  and radius  $0.01 \text{ cm}$ . The separation of the two pinned ends is described by the angle in the horizontal plane, measured from the cylinder axis, and by the angle from the horizontal of a straight line between the pin sites. The three curves represent a bump size of  $3 \mu\text{m}$  with friction coefficients of  $0.5$  (+) and  $5.0$  (□), and a bump size of  $17 \mu\text{m}$  with friction coefficient  $5.0$  (●).

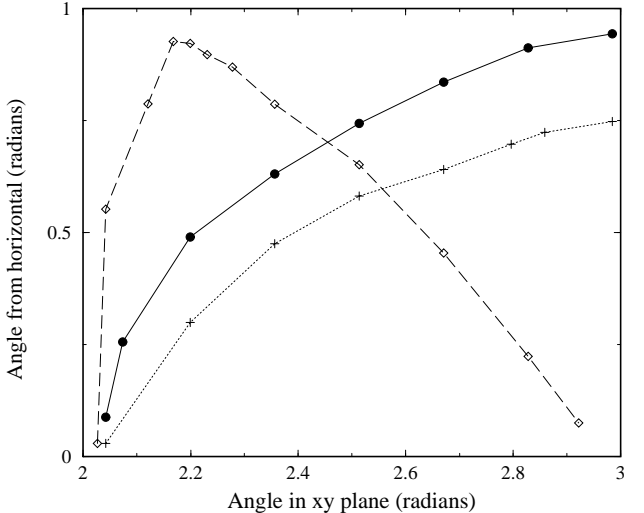


FIG. 11: Stable regime with and without a central vortex. The two pinned ends are separated both horizontally and vertically. The three curves represent no additional fluid flow in the cell (●), an  $N = 1$  vortex at the center (+), and an  $N = -1$  vortex at the center (◇). The vertical component of the pinned vortex is in the same direction as the  $N = 1$  central vortex.

the central vortex and pinned loop have opposite circulation, they attract each other. For horizontal angles near  $0.7\pi$ , this pulls the loop away from the wall and helps stabilize it. As the pinned vortex traverses more of the cell, though, a portion of it must pass too near the central vortex. The  $1/r$  velocity field of the central vortex leads to an instability, attracting the other vortex more and more strongly. Again the final result is a time step crash, in this case caused by the large central velocity field rather than by an attraction to the outer wall. Figure 12 illustrates this situation, which determines the boundary of the stable regime for horizontal angles above  $2.2$  radians.

Another issue of experimental importance is having a substantial vertical component, since typically cryostats rotate only about a vertical axis. Reproducibly creating a mainly horizontal pinned vortex may be difficult under these circumstances, so we examined ways to stabilize more nearly vertical vortices.

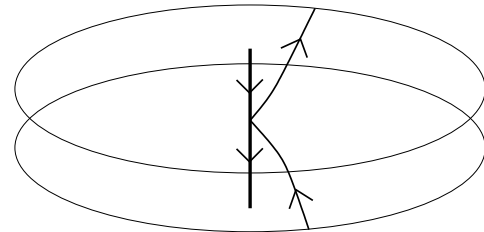


FIG. 12: Vortex line being pulled in to center of cell. The central vortex is directed opposite the vertical component of the vortex pinned to the outer walls.

Imposing a vertical superfluid flow alters the stability regime, as discussed in early work on vortices in channels [18]. For a horizontal vortex, the vertical flow changes the curvature and can pull the vortex away from the wall. If the vertical velocity is too large, the vortex hits the wall on the opposite side of the pin site. For some angles less than  $0.67\pi$ , a range of vertical velocities can stabilize a vortex. An angle of  $0.6\pi$ , for example, supports a stable vortex with vertical velocities from 0.03 cm/s to 0.11 cm/s. However, an external velocity field most strongly affects vortices perpendicular to it. Once the vortex moves out of a horizontal plane, the vertical flow has less stabilizing effect.

We also investigated sharp projections into the cell as potential pinning sites. The calculations discussed above ignore the structure of the pinning center but assume its dimension are small compared to the point spacing. A long spike must be treated slightly differently. We consider two long, thin spikes, aligned vertically with each other. The vortex follows the projections along their lengths, then stretches freely between their ends. We vary both the angle between the projections and the wall, and the length of the projections. Without circulation at the center of the cell, no parameters support a stable vortex. We have tested projections with lengths up to  $\frac{2}{3}$  the cell radius, at angles from  $0.06\pi$  to  $\pi/2$  with the wall. In every case, the center of the vortex line is pulled towards the wall. As it moves, the portions near the projections bend. Eventually the vortex forms a hairpin near the protrusion, and the time step becomes too small to use. We believe an actual vortex would be pulled into the wall and destroyed. A central vortex can stabilize the vortex between the projections, but only when the two have opposite circulation. Thus long spikes are probably not useful pin centers for our experimental purposes.

In the actual experiments, a cell is typically 0.15 cm radius and 5 cm long. As shown earlier, the length is unimportant as long as the cylinder is much longer than it is wide. Furthermore, except for the vortex core size, which appears only in the logarithmic prefactor of the local term, the governing differential equation scales with distance. Since the logarithm produces only a small deviation from perfect scaling, multiplying all length scales by 15 gives reasonable results for a radius 0.15 cm container. For perfect scaling, the angles shown in Figures 10 and 11 would not change with cell size. The maximum bump size represented by the calculations becomes about 0.25 mm, a practical number for deliberately imposed roughness.

We find that in a cylinder, stable macroscopic pinned vortex lines have a limited range of possible configurations, all requiring a large horizontal component. Similar limits on stable vortex configurations apply to other geometries as well. For example, Schwarz noticed that for parallel planes, pin sites not directly opposite each other can support a stable vortex, but with a reduced critical velocity [10]. As the lateral separation increases, the vortex becomes more nearly parallel to the wall, a geometry that pulls the vortex towards its image. We investigated this behavior with our imposed pinning. For a plane separation of 0.02 cm, we find that vortices with at least 0.04 cm lateral displacement are unstable even with no applied velocity field. With real pin centers, the vortex ends

would leave the pins and move closer together, making the vortex more nearly perpendicular to the planes.

The limited possibilities for stable trapped vortices offer at least a partial explanation for the extremely smooth vortex motion observed in experiments [7, 19]. The cryostat rotates to create circulation, but stops before measurements begin. The additional circulation present in the cell during rotation could pin to the walls, as shown in Figure 1. It should then disturb the motion of the detached portion of the central vortex. With many such vortices traversing the cell, the central vortex motion would be irregular. Our work here suggests that large pinned vortices are not common, particularly if the initial circulation is vertical. The limits on vortex configurations may also be relevant to flow experiments in channels and to the problem of remnant vorticity and critical velocities. Vortices pinned to parallel plates have been observed in superfluid helium both before and after rotation [20], but other geometries may be less prone to such pinning of macroscopic vortex lines. Even if pinned vortices are present, there may be significant restrictions on their orientation.

Our calculations have no implications for vortices with length comparable to the cell roughness, believed to create a vortex mesh covering the wall. A vortex pinned between two bumps with radius comparable to their spacing could behave like a vortex line between parallel planes. Without considering the detailed shape of the pinning sites, we cannot address this length scale. Instead, the macroscopic vortices we discuss have stability determined by the large-scale cell geometry.

Since these macroscopic vortices remain far from the wall for most of their length, their behavior may be similar to truly free vortex lines. In future experiments, we hope to study their interaction with a vortex partially trapped on the wire. We have begun to calculate the vortex motion in this experimental setup, for direct comparison with the measurements. In addition, we plan further computational work to search for stable vortex configurations involving multiple vortex lines and vortices of the same scale as the wall roughness. A separate line of work, of less relevance to our own measurements but more applicable to other experiments, would be to study the stability of pinned vortices in a rotating cylinder.

We thank A. Tesdall for his early work on the computer code.

## REFERENCES

- [1] R.J. Donnelly, *Quantized Vortices in Helium II* (Cambridge University Press, Cambridge, 1991).
- [2] C.F. Barenghi, R.J. Donnelly, and W.F. Vinen, “Friction on quantized vortices in helium II: a review,” *J. Low Temp. Phys.* **52**, 189 (1983).
- [3] M.R. Smith, R.J. Donnelly, N. Goldenfeld, and W.F. Vinen, “Decay of vorticity in homogeneous turbulence,” *Phys. Rev. Lett.* **71**, 2583 (1993).
- [4] S.L. Davis, P.C. Hendry, and P.V.E. McClintock, “Decay of quantized vorticity in superfluid  $^4\text{He}$  at mK temperatures,” *Physica B* **280**, 43 (2000).

- [5] M. Abid et al., "Experimental and numerical investigation of low-temperature superfluid turbulence," *Euro. J. Mech. B, Fluids* **17**, 665 (1998).
- [6] C. Nore, M. Abid, and M.E. Brachet, "Kolmogorov turbulence in low-temperature superflows," *Phys. Rev. Lett.* **78**, 3896 (1997); "Decaying Kolmogorov turbulence in a model of superflow," *Phys. Fluids* **9**, 2644 (1997).
- [7] R.J. Zieve et al., "Precession of a single vortex line in superfluid  $^3\text{He}$ ," *Phys. Rev. Lett.* **68**, 1327 (1992); "Investigation of quantized circulation in  $^3\text{He}$ ," *J. Low Temp. Phys.* **91**, 315 (1993).
- [8] R.J. Zieve, J.D. Close, J.C. Davis, and R.E. Packard, "New experiments on the quantum of circulation in  $^4\text{He}$ ," *J. Low Temp. Phys.* **90**, 243 (1993).
- [9] K.W. Schwarz, "Unwinding of a single quantized vortex from a wire," *Phys. Rev.* **B47**, 12030 (1993).
- [10] K.W. Schwarz, "Three-dimensional vortex dynamics in superfluid  $^4\text{He}$ : Line-line and line-boundary interactions," *Phys. Rev.* **B31**, 5782 (1985).
- [11] D.C. Samuels, "Velocity matching and Poiseuille pipe flow of superfluid helium," *Phys. Rev.* **B46**, 11714 (1992).
- [12] M. Tsubota and S. Maekawa, "Pinning and depinning of two quantized vortices in superfluid  $^4\text{He}$ ," *Phys. Rev.* **B47**, 12040 (1993).
- [13] R.G.K.M. Aarts and A.T.A.M. de Waele, "Numerical investigation of the flow properties of He II," *Phys. Rev.* **B50**, 10069 (1994).
- [14] C.F. Barenghi, D.C. Samuels, G.H. Bauer, and R.J. Donnelly, "Superfluid vortex lines in a model of turbulent flow," *Phys. Fluids* **9**, 2631 (1997).
- [15] Ref. 1, pp.213-214.
- [16] K.W. Schwarz, "Vortex pinning in superfluid helium," *Phys. Rev. Lett.* **47**, 251 (1981).
- [17] S.G. Hedge and W.I. Glaberson, "Pinning of superfluid vortices to surfaces," *Phys. Rev. Lett.* **45**, 190 (1980).
- [18] W.I. Glaberson and R.J. Donnelly, "Growth of pinned quantized vortex lines in helium II," *Phys. Rev.* **141**, 208 (1966).
- [19] L. Hough, L.A.K. Donev, and R.J. Zieve, "Smooth vortex precession in superfluid  $^4\text{He}$ ," to be published.
- [20] D.D. Awschalom and K.W. Schwarz, "Observation of a remnant vortex-line density in superfluid helium," *Phys. Rev. Lett.* **52**, 49 (1984).